Diabetes Publish Ahead of Print, published online July 10, 2007

Mitochondrial energetics in the heart in obesity related diabetes: direct evidence for increased uncoupled respiration and activation of uncoupling proteins

Sihem Boudina[1], Sandra Sena[1], Heather Theobald[1], Xiaoming Sheng [2], Jordan J. Wright[1], Xia Xuan Hu [1], Salwa Aziz[1], Josie I. Johnson[1], Heiko Bugger [1],Vlad G. Zaha[1] and E. Dale Abel[1].

[1]Division of Endocrinology, Metabolism and Diabetes and Program in Human Molecular Biology and Genetics, University of Utah School of Medicine, Salt Lake City, Utah 84112.
[2]Department of Family and Preventive Medicine, University of Utah School of Medicine, Salt Lake City, Utah 84112.

Running Title: Mitochondrial Uncoupling in Diabetes

Address correspondence to: E. Dale Abel, Division of Endocrinology, Metabolism and Diabetes, Program in Human Molecular Biology and Genetics, 15 N 2030 East, Bldg # 533 Rm. 3410B, Salt Lake City, Utah 84112, E-Mail: dale.abel@hmbg.utah.edu

Received for publication 7 April 2007 and accepted in revised form 2 July 2007.

Additional information for this article can be found in an online appendix at http://diabetes.diabetesjournals.org.

ABSTRACT

Objective. In obesity and diabetes, myocardial fatty acid (FA) utilization and myocardial oxygen consumption (MVO_2) are increased and cardiac efficiency (CE) is reduced. Mitochondrial uncoupling has been proposed to contribute to these metabolic abnormalities; but has not been directly demonstrated.

Research Design and Methods. Oxygen consumption and cardiac function were determined in *db/db* hearts perfused with glucose or glucose and palmitate. Mitochondrial function was determined in saponin permeabilized fibers and proton leak kinetics and H_2O_2 generation determined in isolated mitochondria.

Results. *db/db* hearts exhibited reduced cardiac function and increased MVO_2. Mitochondrial ROS generation, lipid and protein peroxidation products were increased. Mitochondrial proliferation was increased in *db/db* hearts, oxidative phosphorylation capacity was impaired but H_2O_2 production was increased. Mitochondria from *db/db* mice exhibited FA-induced mitochondrial uncoupling that is inhibitable by GDP suggesting that these changes are mediated by uncoupling proteins. Mitochondrial uncoupling was not associated with an increase in uncoupling protein content, but FAO genes and expression of electron transfer flavoproteins were increased whereas the content of the F1 alpha- subunit of ATP synthase was reduced.

Conclusion. These data demonstrate that mitochondrial uncoupling in the heart in obesity and diabetes is mediated by activation of uncoupling proteins independently of changes in expression levels. This likely occurs on the basis of increased delivery of reducing equivalents from beta-oxidation to the electron transport chain, which coupled with decreased OXPHOS capacity increases ROS production and lipid peroxidation.

INTRODUCTION

Diabetes is associated with altered myocardial substrate metabolism that is believed to contribute to contractile dysfunction. In many studies in rodents and humans there is a characteristic increase in fatty acid (FA) utilization and an accompanying reduction in glucose and lactate utilization (1; 2). Some studies have revealed a reduced ability to enhance FA oxidation in the face of increased lipid delivery, as well as metabolic inflexibility, which might be consistent with mitochondrial dysfunction (3; 4). More recently, evidence has emerged that increased myocardial oxygen consumption (MVO_2) and decreased cardiac efficiency (CE) may also contribute to cardiac dysfunction in obesity and diabetes (5-9). The mechanisms for reduced CE are partially understood but it has been suggested that mitochondrial uncoupling may contribute to this, based upon reduced ATP/O ratios in mitochondria isolated from obese (*ob/ob*) mice following exposure to FA (10), and other studies that have shown increased levels of uncoupling proteins (11).

Uncoupling proteins (UCPs) are inner mitochondrial membrane proteins that play a role in dissipating the mitochondrial proton gradient (12). UCP1-mediated uncoupling of brown adipose tissue is well accepted (13). The biological functions of UCP2 and UCP3, which are expressed in the heart, are still incompletely understood (7; 11; 14-16), but proposed roles include antioxidant defense following ischemia-reperfusion injury (16). Increased UCP2 and UCP3 have been correlated with reduced CE in hypertrophied hyperthyroid hearts (17), and levels of UCP3, which are regulated by fatty acid-mediated PPARα signaling are increased in the hearts of streptozotocin-treated mice and in diabetic *db/db* mice (11). While these studies are consistent with the notion that mitochondrial uncoupling contributes to the altered energy metabolism in diabetic hearts, direct measurements of mitochondrial uncoupling in diabetic hearts is relatively lacking. UCP proteins can be allosterically activated by superoxides (ROS) (18; 19) and ROS byproducts such as carbon-centered radicals (20), hydroperoxy fatty acids (21; 22), and lipid peroxidation products, *e.g.* 4-hydroxy-2-nonenal (4-HNE) (23-25). 4-HNE-induced uncoupling of brown adipose tissue might be UCP1 independent (26), and data exist that other mitochondrial proteins such as the adenine nucleotide translocase (ANT) may mediate oleate and palmitate induced uncoupling in rat heart mitochondria (25; 27; 28).

The goal of the present study was to directly ascertain if mitochondrial uncoupling exists in hearts of diabetic *db/db* mice, to determine if this involves activation of uncoupling proteins or ANT and if so, to determine potential mediators of this activation. FA increased MVO_2 and reduced CE in hearts from hyperglycemic *db/db* mice. Mitochondrial oxidative capacity was reduced despite increased mitochondrial proliferation and hydrogen peroxide generation and the lipid peroxidation products MDA and 4-HNE were increased. FA, uncoupled mitochondrial oxidative metabolism and ATP synthesis. Proton leak was increased in *db/db* mitochondria despite normal UCP3 content and was inhibited by GDP, providing direct evidence that UCPs are activated in mitochondria of the *db/db* model of type 2 diabetes and obesity.

MATERIALS AND METHODS

Animals – Male *db/db* mice (C57BLKS background) and lean C57BLKS controls, obtained from Jackson Laboratories (Bar Harbor, ME) were studied between the ages of 8-9 weeks. At this age *db/db* mice are consistently severely hyperglycemic, and corresponds to the age at which we previously studied substrate metabolism and CE (9). Mice were maintained with 12-h light/12-h dark photoperiods with free access to water and food and studied in accordance with protocols approved by the Institutional Animal Care and Use Committee of the University of Utah. All studies were performed in random-fed animals.

Electron microscopy –Samples, taken from the endocardium of the left ventricle, were fixed in 2.5% glutaraldehyde and 1% paraformaldehyde, post-fixed in 2% osmium, embedded in resin, and sectioned (80-100 nm thick). Morphometric analysis was assessed using blind counting to determine mitochondria number per myofibrillar surface. Three sections from each of three separate hearts per genotype were quantified at magnification of X 8000.

Mitochondrial DNA quantification – DNA was extracted and purified using the DNeasy Tissue Kit (Qiagen Inc., Valencia, CA). Primer pairs were designed using GenBank reference sequences for: cytoplasmic beta actin (ACTB) and mitochondrial cytochrome b (CYTB) (See supplementary table S1 for primer sequences [available at http://diabetes.diabetesjournals.org]).
Real time PCR was performed using an ABI Prism 7900HT instrument (Applied Biosystems, Foster City, CA) in 384-well plate format with SYBR Green I chemistry and ROX internal reference (Invitrogen Corporation, Carlsbad, CA). All reactions were performed in triplicate. Relative quantification was performed by interpolating crossing point data on an independent standard curve thereby accounting for any difference in amplification efficiency. Mitochondrial DNA was expressed relative to nuclear DNA.

Hydrogen peroxide (H_2O_2) levels – Mitochondrial H_2O_2 generation was measured by monitoring H_2O_2-induced-fluorescence of homovanillic acid (λex. 312 nm, λem. 420) under the catalysis of horseradish peroxidase using a spectro-fluorophotometer (RF5301PC, Shimadzu, Columbia, MD) as previously described by Barja (29). Succinate (4mmol/L) was used to stimulate ROS production following inhibition of the F_1F_0-ATP synthase with oligomycin (1 μg/ml). The inhibitor rotenone (10 μmol/L) was then added to the mixture to stop Complex I-mediated superoxide production. Although the readout for this assay is H_2O_2 it is widely accepted that this method assays mitochondrial superoxide production.

Malondialdehyde levels (MDA) –Lipid peroxidation was determined by measuring MDA using a Lipid Peroxidation Assay Kit, (Calbiochem-Novabiochem Corporation, USA).

Perfused Hearts – Cardiac function in the presence or absence of FA was studied in paced (360 beats/minute), isolated hearts from *db/db* and control mice (perfusion pressure of 60mmHg for 20-minutes) using Langendorff retrograde preparations as described before (7).

Mitochondrial function **–** Saponin-permeabilized cardiac fibers isolated from the LV endocardium, were used to measure respiratory parameters of the total mitochondrial population *in situ*, using protocols we previously described (30; 31). Studies were performed in hearts perfused with glucose alone (11 mmol/L), or glucose (11mmol/L) and palmitate (1mmol/L) to mimic the in vivo milieu of *db/db* mice (9). Fibers were exposed to three independent substrates: (in mmol/L) 5 glutamate, 10 pyruvate or 0.02 palmitoyl-carnitine (all with 2 malate). ATP synthesis rates were determined under state 3 conditions by sampling the respiratory buffer every 10-seconds for 60 seconds, immediately after addition of ADP (7). To determine potential mediators of mitochondrial uncoupling, saponin-permeabilized cardiac fibers under state 4 conditions (oligomycin 1 µg/mL) and in the presence of succinate (4 mmol/L), rotenone (10 µmol/L) and either GDP (500 µmol/L) alone or combined with atractyloside (ATR) (5 µmol/L) were analyzed.

Proton leak measurements **–** Mitochondria were prepared from whole hearts by differential centrifugation at 4ºC, and proton leak kinetics measured in succinate-stimulated mitochondria as previously reported (25; 27). Proton leak measurements were performed in hearts that were pre-perfused for 20 min with 11 mmol/L glucose and 1 mmol/L palmitate prebound to 3% (w/v) BSA. Proton leak was measured in the absence (control) or presence of GDP (500 µmol/L) alone or combined with ATR (5 µmol/L).

Western-blot analysis **–** Total or mitochondrial proteins were resolved by SDS-PAGE as described (7). Antibodies used were: mouse anti-Oxphos Complex II (the 30 kDa protein) and anti-Oxphos Complex V (F1 complex, α subunit) (Molecular Probes – Invitrogen, Carlsbad, CA), mouse anti-MnSOD (BD Biosciences, San Jose, CA), rabbit anti-4-Hydroxy-nonenal (4-HNE)-Michael adducts (Calbiochem, La Jolla, CA), rabbit anti-UCP3 (Affinity Bioreagents, Golden, CO), and rabbit polyclonal anti-ANT1serum (provided by Douglas Wallace, University of California Irvine). For loading controls, mouse anti-α tubulin (Sigma, Saint Louis, MO) was used for heart proteins and Coomassie Blue R-250 (Biorad, Hercules, CA) staining for mitochondrial proteins. UCP 3KO and ANT1KO heart lysates were used as negative controls for UCP3 and ANT1 western blots.

RNA extraction and quantitative RT-PCR **–** Total RNA was extracted from hearts with Trizol reagent (Invitrogen Corporation, Carlsbad, CA), purified with the RNEasy Kit (Qiagen Inc., Valencia, CA) and reverse transcribed. Equal amounts of cDNA from the hearts of six mice were subjected to real-time PCR as described for mitochondrial DNA. Data were normalized by expressing them relative to the levels of the invariant transcript Lamin A (LMNA).

Statistical analysis **–** Data are means ± SEM. Significance was determined by ANOVA followed by Fisher's least protected squares test using Statview 5.0.1 software (SAS Institute, Cary, NC). Nonparametric Mann Witney test was used to compare cardiac efficiency between glucose-perfused *db/db* and wildtype hearts. Proton leak curves were log-transformed so that a general linear model is applicable. Comparisons of the slopes and intercepts were determined by a t-test and $p < 0.05$ was considered significant.

RESULTS

Cardiac function in Langendorff-perfused hearts.

Heart weights were not different between the two groups (Table I). In glucose-perfused *db/db* hearts, left ventricular developed pressure (LVDP) and rate pressure product (RPP) were significantly reduced ($p < 0.05$). MVO_2 was unchanged, thus cardiac efficiency (CE) was lower in *db/db* mice versus controls ($p < 0.05$). Similar to previous reports (6; 7) perfusion with glucose and palmitate reduced contractile function (systolic pressure, LVDP and RPP) in wildtypes and MVO_2 proportionately decreased (Table I) so that CE was similar in glucose and glucose + palmitate-perfused control hearts. FA exposure caused a greater decline in contractile function in *db/db* hearts (Table I). Compared to equivalently perfused wildtype hearts, MVO_2 was 1.4 ± 0.1-fold higher in glucose + palmitate-perfused *db/db* hearts resulting in a 50.6 ± 7.2 % reduction in CE (Table I).

Mitochondrial biogenesis is increased in db/db hearts

By electron microscopy, ultrastructure of sarcomeric units in *db/db* hearts was not grossly different from wildtypes except for increased intracellular lipid droplets in *db/db* hearts (Figure 1A and supplementary Figure S5). Cardiac steatosis was also confirmed by oil-red-O staining (Supplementary Figure S5) and by direct measurement of myocardial triglyceride content which was 2.2 fold higher in *db/db* hearts (7.4 ± 1 vs. 16.3 ± 1.4 μmol.g wet heart weight^{-1}, $P < 0.005$). Evidence for mitochondrial biogenesis was also observed (Figure 1A). Mitochondrial number was 1.36 ± 0.1 fold and mitochondrial DNA copy 1.4 ± 0.09 fold higher in *db/db* hearts (Figure 1B and 1C). Mitochondrial volume density was also increased by 18% in *db/db* hearts (45.5% ± 3.6% vs. 37.6% ± 2.1 %; $p < 0.05$). The fold-increase in volume density was ~ 50% of the increase in mitochondrial number, therefore indicating that the mitochondrial biogenic response in the *db/db* heart is associated with mitochondria that are somewhat smaller.

Increased Hydrogen Peroxide Generation and Peroxidation Products in db/db Hearts

In the presence of oligomycin alone, H_2O_2 generation was not increased in *db/db* mitochondria. Succinate increased H_2O_2 production to a greater extent in *db/db* mitochondria (0.55 ± 0.11 versus 0.31 ± 0.06 μM/min/mg mitochondrial proteins, $p < 0.01$). Rotenone (Complex I Inhibitor) reduced H_2O_2 production by 52% in wildtypes and by 39% in *db/db* hearts (Figure 2A), so that H_2O_2 generation remained 2.3-fold greater in *db/db* mitochondria than similarly treated wildtypes ($p = 0.06$), and was significantly increased relative to *db/db* mitochondria exposed to oligomycin alone ($p < 0.03$). In contrast, rotenone returned H_2O_2 generation in wildtypes to levels that were unchanged relative to mitochondria exposed to oligomycin alone ($p = 0.3$). Thus Complex I is the major source of ROS in succinate-treated mitochondria from wildtypes, whereas ROS production in *db/db* mitochondria arises not only from Complex I but from additional complexes. Mitochondrial ROS generation was associated with increased lipid and protein peroxidation. Malondialdehyde (MDA) (1.2 ± 0.01 fold ($p < 0.005$)) and 4-HNE protein adducts ($p < 0.05$) were increased in *db/db* hearts (Figure 2B and 2C) despite a modest increase in mitochondrial superoxide dismutase protein (Figure 2C).

Reduced Mitochondrial Function in Glucose-Perfused db/db hearts

In saponin-permeabilized fibers isolated from glucose-perfused hearts, state 2 (V_0) and ADP-stimulated respiration rates (state 3 –V_{ADP}) with glutamate, pyruvate and palmitoyl-carnitine (PC) were depressed in *db/db* hearts (Figure 3A, B and C). ATP synthesis rates were proportionately reduced in *db/db* hearts by 58.1 ± 5.3 % and 35.9 ± 4.8 % with glutamate and pyruvate respectively (Figure 3D and 3E) so that ATP/O ratios were not different from controls for any substrate (Figure 3D, E and F). Reduced ATP synthesis is unlikely due to differences in endogenous ATPases, as ATP hydrolysis rates were not increased in *db/db* fibers (Supplementary Figure S2). We then measured protein levels of several subunits of the electron transport chain: Complex I (subunit 9), Complex II (30 kDa protein), Complex III (core I), and Complex V (F1 complex, α subunit). Complex I, II and III protein levels were unchanged in *db/db* hearts (data not shown). However, levels of the α-subunit of the F1 ATP synthase complex were reduced by 41% ± 3% in *db/db* hearts ($p < 0.05$) (Figure 3G).

Mitochondria from FA-perfused db/db Mouse Hearts are Uncoupled

Mitochondria from *db/db* hearts examined after palmitate + glucose perfusion showed increased state 4 (V_{Oligo}) respirations with palmitoyl-carnitine (PC) compared to similarly perfused controls (Figure 4B). State 3 (V_{ADP}) respirations which were reduced in glucose perfused *db/db* hearts actually increased following perfusion with palmitate + glucose (13.06 ± 0.9 vs. 16.38 ± 1.27 $nmolO_2.min^{-1}.mg\ dry\ weight^{-1}$, $p = 0.05$) (Figure 4A). This contrasts with state 3 (V_{ADP}) respiration rates from wildtype fibers which were reduced slightly following palmitate + glucose perfusion. Despite increased state 3 respirations, ATP production was lower in *db/db* hearts (figure 4C) and ATP/O ratios were reduced by 36 ± 7 % (Figure 4D), consistent with FA-mediated mitochondrial uncoupling in *db/db* mouse hearts.

FA-induced Mitochondrial Uncoupling is Mediated in Part by Uncoupling Proteins

Cardiac fibers from FA perfused *db/db* hearts were studied under state 4 conditions in the presence of succinate and rotenone (an inhibitor of Complex 1) in the presence or absence of specific inhibitors of uncoupling proteins (GDP) and the adenine nucleotide translocase (atractyloside: ATR). Prior to the addition of GDP or ATR, oxygen consumption was similar in both groups of mice, suggesting equivalently uncoupled respirations under these conditions. GDP reduced respiration rates in *db/db* and controls ($p < 0.001$). Interestingly, in the presence of GDP, O_2 consumption remained 37% higher in *db/db* compared to controls (8.1 ± 0.8 vs. 5.9 ± 0.6 $nmol.min^{-1}.mg\ dry\ weight^{-1}$, $p = 0.05$) (Figure 5A). Addition of atractyloside (ATR) abolished this increase in *db/db* but had no additional effect in controls, suggesting that ANT may mediate a component of the mitochondrial uncoupling observed in *db/db* mitochondria.

We next performed proton leak kinetics analyses in mitochondria isolated from glucose + palmitate-perfused hearts to more directly evaluate mitochondrial uncoupling. (See supplementary data, Table S2 and S3, for mean ± SEM for all proton leak experiments and log transformed regression equations). Figures 5B –5F illustrate proton leak kinetics prior to and after the serial addition of GDP and ATR. Addition of GDP did not alter proton leak kinetics in wildtype mitochondria.

Intriguingly, a leftward shift in the wildtype proton leak curve ($p < 0.03$ for intercepts) suggested that ATR increased proton leak in wildtype mitochondria (Figure 5B). In contrast, treatment with GDP reduced proton leak in *db/db* mitochondria, (rightward shift in proton leak curves, $p < 0.002$ for slope and intercept, Figure 5C). In the presence of GDP + ATR, proton leak remained significantly different from untreated *db/db* mitochondria ($p < 0.04$, for intercepts), and tended to be shifted to the right versus GDP alone ($p = 0.08$ for slope and $P = 0.1$ for intercept, Figure 5C). Figures 5 D-F compare proton leak kinetics between wildtype and *db/db* mitochondria under similar treatment conditions. In the absence of inhibitors (GDP and ATR) *db/db* mitochondria (red circles) exhibit increased proton leak (Figure 5D) particularly at membrane potentials < 150 mV ($p < 0.05$ and $p < 0.03$ respectively for slopes and intercepts). GDP had no effect in controls but shifted *db/db* curves to the right (Figures 5B and C) restoring proton leak to wildtype levels. Because ATR had opposite effects in *db/db* and wildtype mitochondria, in the presence of GDP and ATR, intercepts of the proton leak kinetics curves were different ($p < 0.02$) (Figure 5F). Taken together these data indicate that proton leak is increased in *db/db* mitochondria and is mediated to a large extent by activation of uncoupling proteins, with a small component mediated by ANT.

UCP 3, ANT1 protein expression, and Gene Expression Analyses

UCP 3 protein was not increased in *db/db* hearts (Figure 6A), nor was there any difference in mRNA levels of UCP2 (Figure 7). ANT proteins were 33% lower in *db/db* relative to controls (Figure 6B). Thus mitochondrial uncoupling likely occurs via increased activation that is independent of changes in protein levels. Additional genes were measured to explore transcriptional mechanisms that might further elucidate mechanisms responsible for the FA-mediated uncoupling in *db/db* mitochondria (Figure 7). Expression levels of MCAD, LCAD, PPAR-α, HADHA, HADHB, MTE1 and PGC1-α were increased in *db/db* hearts, consistent with roles in activating FAO and increasing mitochondrial biogenesis. Despite increased PPAR-α gene expression, UCP3 expression was reduced ($p < 0.05$), UCP2 levels were unchanged and ANT1 expression trended upwards in *db/db* hearts ($p = 0.08$). The expression of electron transfer flavoprotein (ETF) subunits alpha and beta (ETFA and ETFB) that deliver reducing equivalents generated in beta-oxidation to the electron transport chain were increased in *db/db* hearts. In contrast, there was no coordinate increase in OXPHOS subunit, gene expression.

DISCUSSION

We have performed a comprehensive analysis of the mitochondrial phenotype in the hearts of *db/db* mice, a model of obesity and severe type 2 diabetes. Our study yielded a number of novel observations. Diabetes and obesity is associated with mitochondrial proliferation in the heart. This observation is consistent with a recent study showing increased mitochondrial proliferation in insulin resistant UCP-DTA mice (32). This mitochondrial proliferation in *db/db* hearts may be driven in part by increased expression of PGC1-α. Although an increase in PGC1-α and PPAR-α signaling may promote increased expression of FAO genes, and although increased expression of electron transfer flavoprotein genes may increase the

delivery of reducing equivalents to the electron transport chain, there is not a uniform upregulation of OXPHOS gene expression. These findings are consistent with the hypothesis that increased delivery of reducing equivalents from FA oxidation coupled with reduced ability to completely oxidize these equivalents might contribute to increased mitochondrial ROS generation, which leads to mitochondrial uncoupling. In isolated hearts, addition of FA to perfusates increases oxygen consumption in *db/db* hearts without a proportionate increase in cardiac work. While *db/db* mitochondria exhibit reduced oxidative capacity they become significantly uncoupled in fibers isolated from hearts that were exposed to FA. Uncoupling was further supported by increased proton leak mediated predominantly by activation of UCPs, with minor contributions from ANT that were independent of increased protein levels. Mitochondrial uncoupling may initially represent an adaptative response to increased FA oxidation and FA-mediated ROS generation, however it does not completely normalize mitochondrial ROS overproduction as evidenced by accumulation of lipid peroxidation products such as MDA and 4HNE. Moreover, it could also be argued that the negative impact of mitochondrial uncoupling to reduce mitochondrial ATP supply might ultimately prove to be maladaptive in terms of maintaining myocardial high-energy phosphate reserves.

Mitochondrial biogenesis represents an adaptive mechanism by which oxidative capacity can be increased in tissues in response to various stimuli. In hearts, upregulation of PGC-1α-mediated signaling plays an important role in metabolic maturation from infancy to adulthood and in increasing FA oxidative capacity in response to physiological cardiac hypertrophy as occurs during development or after exercise (33; 34) and (Abel ED, unpublished observations). In these contexts PGC-1α increases oxidative capacity and mitochondrial anti-oxidant defense mechanisms (35). Cardiac mitochondrial biogenesis has been described in a mouse model of type 1 diabetes (36) and we now show that this also occurs in obesity and type-2 diabetes. Whereas these mitochondrial changes might be driven in part by increased PGC1-α, they are not associated with a coordinate increase in OXPHOS subunit gene expression or increased mitochondrial oxidative capacity. Moreover, increased ROS production coupled with increased protein and lipid peroxidation implies that ROS defenses in these diabetic hearts were not sufficiently increased to circumvent the increased oxidant burden. A number of potential mechanisms might contribute to this maladaptive phenotype. First, increased PPAR-α expression coupled with increased delivery of FA ligands might activate FAO pathways disproportionately in *db/db* hearts (37; 38). Second it is possible that additional transcriptional targets must be activated in order to fully execute a coordinated response to increased PGC-1α expression. Support for this comes from studies in which forced overexpression of PGC-1α in the heart leads to mitochondrial biogenesis that is maladaptive (39; 40). The specific nature of these additional factors remains to be determined, and we would hypothesize that activation of these pathways are impaired in the diabetic heart.

The present study confirms the existence of oxidative stress in diabetic hearts (41-44). Direct evidence is provided that mitochondria are a likely source of increased ROS, given increased H_2O_2

production in *db/db* mitochondria. Complex I contributes to succinate-induced mitochondrial ROS generation in wildtype and *db/db* mitochondria. In contrast, a significant increase in ROS generation persisted in rotenone-treated *db/db* mitochondria. This would suggest that additional downstream mechanisms contribute to increased ROS generation in *db/db* mitochondria. Gene expression studies raise the possibility that increased transfer of electrons from reducing equivalents generated by beta-oxidation and succinate could contribute to increased mitochondrial ROS generation in *db/db* mitochondria downstream of Complex I. ETFA (Electron transfer flavoprotein, α subunit), ETFB (Electron transfer flavoprotein, β subunit and ETFQO (Electron transfer flavoprotein-ubiquinone oxidoreductase) play an important role in electron transfer between Acyl-CoA substrates to Ubiquinone (UQ) (45) linking the oxidation of fatty acids and some amino acids to the mitochondrial respiratory system. The electron flow can be summarized as follows: Acyl-CoA ™ Acyl-CoA dehydrogenases ™ ETF (A/B) ™ ETFQO ™ UQ ™ complex III (46). Thus, increased delivery of electrons to Complex III in FA perfused *db/db* hearts, coupled with reduced activity of ATP synthase could contribute to increased ROS generation at or downstream of Complex III. Mitochondria are also targets of oxidative damage in the hearts of diabetic animal models (36; 47), which could also contribute to the impaired mitochondrial function observed.

We observed two distinct mitochondrial functional defects in *db/db* mice. By removing the confounding effects of FA, a significant defect in mitochondrial oxidative capacity was revealed in glucose-perfused *db/db* mouse hearts due in part to reduced expression of the α-subunit of the F1 complex of ATP synthase. Although protein levels of selected subunits of the electron transport chain were unaltered, we cannot exclude reduction in activity of other complexes. Second, mitochondrial uncoupling was evident only after palmitate perfusion of *db/db* hearts. Potential mechanisms for FA-mediated mitochondrial uncoupling include upregulation of beta-oxidation pathways and increased capacity of *db/db* hearts to metabolize FA (6; 7; 9), leading to increased generation of the reducing equivalents $FADH_2$, and NADH; increased expression of electron transfer flavoproteins which could increase the delivery of electrons from these reducing equivalents to the electron transport chain, thereby increasing ROS production that activates uncoupling proteins. Additional changes in Complex I and III in *db/db* hearts likely also increase ROS generation as well.

Importantly our proton leak studies show that uncoupling mechanisms are activated in *db/db* hearts despite the lack of a significant increase in the expression levels of UCPs and ANT. Using specific inhibitors we show that mitochondrial uncoupling in *db/db* hearts was GDP sensitive, implicating uncoupling proteins. Future studies using UCP3 or UCP2 null animals will be required to determine which UCP isoform(s) mediate these effects. Atractyloside had a small additive effect, suggesting that ANT may also play a role in FA-mediated uncoupling in *db/db* mouse hearts. These data support the existence of activators of proton conductance that were present only in the hearts of diabetic animals, which activate UCPs and/ANT leading to mitochondrial uncoupling. Our data suggests that these activators could be

increased ROS and increased levels of oxidative products such as 4-HNE, which have been shown to contribute to mitochondrial uncoupling via ANT and UCPS (18; 25). Others have suggested that uncoupling protein expression levels are increased in the hearts of various models of diabetes including *db/db* mice (11). Although the basis for the lack of increased uncoupling protein or gene expression levels in our hands are not immediately obvious, our observations that uncoupling mechanisms are clearly activated in these mice would indicate that in those instances where uncoupling protein content is also increased, then the combination of increased uncoupling protein content and increased activation should have a synergistic effect.

Recent studies in mice and humans have confirmed that cardiac efficiency (CE) is reduced in obesity and diabetes. In some studies, this has been associated with decreased cardiac function (6; 7; 9), and in others with preserved cardiac function (5; 8). However in all of these studies FA oxidation and myocardial oxygen consumption (MVO_2) were increased. The present studies confirm that CE is reduced in *db/db* hearts perfused with either glucose or glucose + FA. The reduction in CE in glucose-perfused *db/db* hearts might reflect the mobilization of the endogenous triglyceride pool, which is increased in these hearts (48). Addition of palmitate reduces cardiac efficiency even further in *db/db* mice, which we postulate is due to mitochondrial uncoupling, which would further limit myocardial ATP supply. Our analyses of ex-vivo cardiac function revealed impaired contractile function in 9-week-old *db/db* mouse hearts. Echocardiography revealed no significant differences in *in vivo* cardiac function of these mice (data not shown). The absence of significant contractile dysfunction in vivo is consistent with a number of studies that have indicated that there is an age-related impairment in function in *db/db* hearts (9). Systolic and diastolic dysfunction by echocardiography are present in 12-week-old but not in 6-week-old mice (49). Using gated MR imaging analysis in *db/db* mice at 5, 9, 13,17 and 22-weeks of age, increased end-diastolic-volume developed only at 13-weeks, impaired LV contractility (PV loop analysis) at 15-weeks and reduced LV Ejection fraction at 22-weeks (50). Using micro-tipped conductance catheters, Van den Bergh et al. observed impaired load-independent LV function in 24-week but not in 12-week-old *db/db* mice, whereas conventional load-dependent parameters such as dP/dt were normal at both ages because of increased preload and decreased afterload (51). Thus the present study demonstrating mitochondrial uncoupling in 9-week-old *db/db* mice and our prior report indicating that reduced CE may occur in isolated hearts as early as 4-weeks of age (9), indicate that altered myocardial energetics are an early characteristic of these hearts, which can be detected using *in vitro* preparations that clearly precede measurable alterations in *in vivo* cardiac function.

In conclusion, this study provides important new information regarding the multiple mechanisms that impair mitochondrial energetics in the heart in diabetes and obesity and provide direct evidence that mitochondrial uncoupling does occur in diabetic hearts. We propose that mitochondrial uncoupling may represent an important mechanism by which diabetic hearts may initially adapt to the characteristic increase in myocardial FA metabolism and increased oxidative stress with the untoward consequence of reduced

cardiac efficiency, and lower ATP generation. Defective energy metabolism in the heart is likely to impair energy requiring processes in the heart such as diastolic relaxation and may increase the susceptibility of diabetic hearts to injury in the context of ischemia and cardiac hypertrophy.

ACKNOWLEDGMENTS

This work was supported by grants RO1HL73167 and UO1HL70525 from the National Institutes of Health, and the Ben and Iris Margolis Foundation to E. Dale Abel who is an Established Investigator of the American Heart Association. S. Boudina was supported by a postdoctoral fellowship from the Juvenile Diabetes Foundation and Vlad Zaha by a post-doctoral fellowship from the American Heart Association. We thank Dr. Bradford B. Lowell for providing us with UCP 3 knockout mice. We acknowledge Prof. Douglas C. Wallace for providing hearts from ANT knockout mice and ANT1 antiserum and Adrian Flier for technical support with the ANT western-blot. Finally, this paper is dedicated to the memory of one of the co-authors Josie I. Johnson, whose life was prematurely cut short in a biking accident prior to the publication of these studies.

.

ABBREVIATIONS

The abbreviations used are: ATR, atractyloside; ANT, Adenine Nucleotide Translocase; FA, fatty acid; CD 36, fatty acid translocase; CE, cardiac efficiency; COX4i1, cytochrome C oxidase subunit IV isoform 1; MVO_2, myocardial oxygen consumption; LVDP, left ventricular developed pressure; RPP, rate pressure product; UCP, Uncoupling Proteins; ETFA, electron transfer flavoprotein α subunit; ETFB, electron transfer flavoprotein β subunit; ETFQO, electron transfer flavoprotein ubiquinone oxidoreductase; HDHA/B, hydroxyacyl CoA dehydrogenase alpha or beta subunit; LCAD, long chain acyl CoA dehydrogenase; LV. Left Ventricle; MCAD, medium chain acyl CoA dehydrogenase; MTE 1, mitochondrial acyl-CoA thioesterase 1; NDUFA9, NADH dehydrogenase (ubiquinone) 1 alpha subcomplex 9; NDUFV1, NADH dehydrogenase (ubiquinone) flavoprotein 1; NRF1, nuclear respiratory factor 1; PPAR-α, peroxisome proliferator activated receptor alpha; PGC-1α, PPAR gamma coactivator 1 α; TFAM, mitochondrial transcription factor A; UCP2/3, Uncoupling protein 2/3; UQCRC, ubiquinol-cytochrome c reductase core protein 1

REFERENCES

1. Boudina S, Abel ED: Diabetic Cardiomyopathy Revisited. *Circulation* 115:3213-3223, 2007

2. Severson DL: Diabetic cardiomyopathy: recent evidence from mouse models of type 1 and type 2 diabetes. *Can J Physiol Pharmacol* 82:813-823, 2004

3. Oakes ND, Thalen P, Aasum E, Edgley A, Larsen T, Furler SM, Ljung B, Severson D: Cardiac metabolism in mice: tracer method developments and in vivo application revealing profound metabolic inflexibility in diabetes. *Am J Physiol Endocrinol Metab* 290:E870-881, 2006

4. Young ME, Guthrie PH, Razeghi P, Leighton B, Abbasi S, Patil S, Youker KA, Taegtmeyer H: Impaired long-chain fatty acid oxidation and contractile dysfunction in the obese Zucker rat heart. *Diabetes* 51:2587-2595, 2002

5. Peterson LR, Herrero P, Schechtman KB, Racette SB, Waggoner AD, Kisrieva-Ware Z, Dence C, Klein S, Marsala J, Meyer T, Gropler RJ: Effect of obesity and insulin resistance on myocardial substrate metabolism and efficiency in young women. *Circulation* 109:2191-2196, 2004

6. Mazumder PK, O'Neill BT, Roberts MW, Buchanan J, Yun UJ, Cooksey RC, Boudina S, Abel ED: Impaired cardiac efficiency and increased fatty acid oxidation in insulin-resistant ob/ob mouse hearts. *Diabetes* 53:2366-2374, 2004

7. Boudina S, Sena S, O'Neill BT, Tathireddy P, Young ME, Abel ED: Reduced mitochondrial oxidative capacity and increased mitochondrial uncoupling impair myocardial energetics in obesity. *Circulation* 112:2686-2695, 2005

8. How OJ, Aasum E, Severson DL, Chan WY, Essop MF, Larsen TS: Increased myocardial oxygen consumption reduces cardiac efficiency in diabetic mice. *Diabetes* 55:466-473, 2006

9. Buchanan J, Mazumder PK, Hu P, Chakrabarti G, Roberts MW, Jeong Yun U, Cooksey RC, Litwin SE, Abel ED: Reduced Cardiac Efficiency and Altered Substrate Metabolism Precedes the Onset of Hyperglycemia and Contractile Dysfunction in two Mouse Models of Insulin Resistance and Obesity. *Endocrinology*, 2005

10. Boudina S, Abel ED: Mitochondrial uncoupling: a key contributor to reduced cardiac efficiency in diabetes. *Physiology (Bethesda)* 21:250-258, 2006

11. Murray AJ, Panagia M, Hauton D, Gibbons GF, Clarke K: Plasma Free Fatty Acids and Peroxisome Proliferator-Activated Receptor {alpha} in the Control of Myocardial Uncoupling Protein Levels. *Diabetes* 54:3496-3502, 2005

12. Klingenberg M, Huang SG: Structure and function of the uncoupling protein from brown adipose tissue. *Biochim Biophys Acta* 1415:271-296, 1999

13. Nicholls DG, Locke RM: Thermogenic mechanisms in brown fat. *Physiol Rev* 64:1-64, 1984

14. Durgan DJ, Hotze MA, Tomlin TM, Egbejimi O, Graveleau C, Abel ED, Shaw CA, Bray MS, Hardin PE, Young ME: The intrinsic circadian clock within the cardiomyocyte. *Am J Physiol Heart Circ Physiol* 289:H1530-1541, 2005

15. Essop MF, Razeghi P, McLeod C, Young ME, Taegtmeyer H, Sack MN: Hypoxia-induced decrease of UCP3 gene expression in rat heart parallels metabolic gene switching but fails to affect mitochondrial respiratory coupling. *Biochem Biophys Res Commun* 314:561-564, 2004

16. McLeod CJ, Aziz A, Hoyt RF, Jr., McCoy JP, Jr., Sack MN: Uncoupling proteins 2 and 3 function in concert to augment tolerance to cardiac ischemia. *J Biol Chem* 280:33470-33476, 2005
17. Boehm EA, Jones BE, Radda GK, Veech RL, Clarke K: Increased uncoupling proteins and decreased efficiency in palmitate-perfused hyperthyroid rat heart. *Am J Physiol Heart Circ Physiol* 280:H977-983, 2001
18. Echtay KS, Roussel D, St-Pierre J, Jekabsons MB, Cadenas S, Stuart JA, Harper JA, Roebuck SJ, Morrison A, Pickering S, Clapham JC, Brand MD: Superoxide activates mitochondrial uncoupling proteins. *Nature* 415:96-99, 2002
19. Negre-Salvayre A, Hirtz C, Carrera G, Cazenave R, Troly M, Salvayre R, Penicaud L, Casteilla L: A role for uncoupling protein-2 as a regulator of mitochondrial hydrogen peroxide generation. *Faseb J* 11:809-815, 1997
20. Murphy MP, Echtay KS, Blaikie FH, Asin-Cayuela J, Cocheme HM, Green K, Buckingham JA, Taylor ER, Hurrell F, Hughes G, Miwa S, Cooper CE, Svistunenko DA, Smith RA, Brand MD: Superoxide activates uncoupling proteins by generating carbon-centered radicals and initiating lipid peroxidation: studies using a mitochondria-targeted spin trap derived from alpha-phenyl-N-tert-butylnitrone. *J Biol Chem* 278:48534-48545, 2003
21. Goglia F, Skulachev VP: A function for novel uncoupling proteins: antioxidant defense of mitochondrial matrix by translocating fatty acid peroxides from the inner to the outer membrane leaflet. *Faseb J* 17:1585-1591, 2003
22. Jaburek M, Miyamoto S, Di Mascio P, Garlid KD, Jezek P: Hydroperoxy fatty acid cycling mediated by mitochondrial uncoupling protein UCP2. *J Biol Chem* 279:53097-53102, 2004
23. Brand MD, Affourtit C, Esteves TC, Green K, Lambert AJ, Miwa S, Pakay JL, Parker N: Mitochondrial superoxide: production, biological effects, and activation of uncoupling proteins. *Free Radic Biol Med* 37:755-767, 2004
24. Esteves TC, Brand MD: The reactions catalysed by the mitochondrial uncoupling proteins UCP2 and UCP3. *Biochim Biophys Acta* 1709:35-44, 2005
25. Echtay KS, Esteves TC, Pakay JL, Jekabsons MB, Lambert AJ, Portero-Otin M, Pamplona R, Vidal-Puig AJ, Wang S, Roebuck SJ, Brand MD: A signalling role for 4-hydroxy-2-nonenal in regulation of mitochondrial uncoupling. *Embo J* 22:4103-4110, 2003
26. Shabalina IG, Petrovic N, Kramarova TV, Hoeks J, Cannon B, Nedergaard J: UCP1 and defense against oxidative stress. 4-Hydroxy-2-nonenal effects on brown fat mitochondria are uncoupling protein 1-independent. *J Biol Chem* 281:13882-13893, 2006
27. Brand MD, Pakay JL, Ocloo A, Kokoszka J, Wallace DC, Brookes PS, Cornwall EJ: The basal proton conductance of mitochondria depends on adenine nucleotide translocase content. *Biochem J* 392:353-362, 2005
28. Schonfeld P: Does the function of adenine nucleotide translocase in fatty acid uncoupling depend on the type of mitochondria? *FEBS Lett* 264:246-248, 1990
29. Barja G: Mitochondrial oxygen radical generation and leak: sites of production in states 4 and 3, organ specificity, and relation to aging and longevity. *J Bioenerg Biomembr* 31:347-366, 1999

30. Saks VA, Veksler VI, Kuznetsov AV, Kay L, Sikk P, Tiivel T, Tranqui L, Olivares J, Winkler K, Wiedemann F, Kunz WS: Permeabilized cell and skinned fiber techniques in studies of mitochondrial function in vivo. *Mol Cell Biochem* 184:81-100, 1998
31. Veksler VI, Kuznetsov AV, Sharov VG, Kapelko VI, Saks VA: Mitochondrial respiratory parameters in cardiac tissue: a novel method of assessment by using saponin-skinned fibers. *Biochim Biophys Acta* 892:191-196, 1987
32. Duncan JG, Fong JL, Medeiros DM, Finck BN, Kelly DP: Insulin-resistant heart exhibits a mitochondrial biogenic response driven by the peroxisome proliferator-activated receptor-alpha/PGC-1alpha gene regulatory pathway. *Circulation* 115:909-917, 2007
33. Huss JM, Kelly DP: Mitochondrial energy metabolism in heart failure: a question of balance. *J Clin Invest* 115:547-555, 2005
34. Burelle Y, Wambolt RB, Grist M, Parsons HL, Chow JC, Antler C, Bonen A, Keller A, Dunaway GA, Popov KM, Hochachka PW, Allard MF: Regular exercise is associated with a protective metabolic phenotype in the rat heart. *Am J Physiol Heart Circ Physiol* 287:H1055-1063, 2004
35. St-Pierre J, Drori S, Uldry M, Silvaggi JM, Rhee J, Jager S, Handschin C, Zheng K, Lin J, Yang W, Simon DK, Bachoo R, Spiegelman BM: Suppression of reactive oxygen species and neurodegeneration by the PGC-1 transcriptional coactivators. *Cell* 127:397-408, 2006
36. Shen X, Zheng S, Thongboonkerd V, Xu M, Pierce WM, Jr., Klein JB, Epstein PN: Cardiac mitochondrial damage and biogenesis in a chronic model of type 1 diabetes. *Am J Physiol Endocrinol Metab* 287:E896-905, 2004
37. Finck BN, Lehman JJ, Leone TC, Welch MJ, Bennett MJ, Kovacs A, Han X, Gross RW, Kozak R, Lopaschuk GD, Kelly DP: The cardiac phenotype induced by PPARalpha overexpression mimics that caused by diabetes mellitus. *J Clin Invest* 109:121-130, 2002
38. Finck BN, Han X, Courtois M, Aimond F, Nerbonne JM, Kovacs A, Gross RW, Kelly DP: A critical role for PPARalpha-mediated lipotoxicity in the pathogenesis of diabetic cardiomyopathy: modulation by dietary fat content. *Proc Natl Acad Sci U S A* 100:1226-1231, 2003
39. Lehman JJ, Barger PM, Kovacs A, Saffitz JE, Medeiros DM, Kelly DP: Peroxisome proliferator-activated receptor gamma coactivator-1 promotes cardiac mitochondrial biogenesis. *J Clin Invest* 106:847-856, 2000
40. Russell LK, Mansfield CM, Lehman JJ, Kovacs A, Courtois M, Saffitz JE, Medeiros DM, Valencik ML, McDonald JA, Kelly DP: Cardiac-specific induction of the transcriptional coactivator peroxisome proliferator-activated receptor gamma coactivator-1alpha promotes mitochondrial biogenesis and reversible cardiomyopathy in a developmental stage-dependent manner. *Circ Res* 94:525-533, 2004
41. Hsieh RH, Lien LM, Lin SH, Chen CW, Cheng HJ, Cheng HH: Alleviation of oxidative damage in multiple tissues in rats with streptozotocin-induced diabetes by rice bran oil supplementation. *Ann N Y Acad Sci* 1042:365-371, 2005
42. Minamiyama Y, Bito Y, Takemura S, Takahashi Y, Kodai S, Mizuguchi S, Nishikawa Y, Suehiro S, Okada S: Calorie Restriction Improves Cardiovascular Risk Factors via Reduction of Mitochondrial Reactive Oxygen Species in Type II Diabetic Rats. *J Pharmacol Exp Ther* 320:535-543, 2007

43. Rosen P, Osmers A: Oxidative Stress in Young Zucker Rats with Impaired Glucose Tolerance is Diminished by Acarbose. *Horm Metab Res* 38:575-586, 2006
44. Ye G, Metreveli NS, Donthi RV, Xia S, Xu M, Carlson EC, Epstein PN: Catalase protects cardiomyocyte function in models of type 1 and type 2 diabetes. *Diabetes* 53:1336-1343, 2004
45. Ramsay RR, Steenkamp DJ, Husain M: Reactions of electron-transfer flavoprotein and electron-transfer flavoprotein: ubiquinone oxidoreductase. *Biochem J* 241:883-892, 1987
46. Zhang J, Frerman FE, Kim JJ: Structure of electron transfer flavoprotein-ubiquinone oxidoreductase and electron transfer to the mitochondrial ubiquinone pool. *Proc Natl Acad Sci U S A* 103:16212-16217, 2006
47. Shen X, Zheng S, Metreveli NS, Epstein PN: Protection of cardiac mitochondria by overexpression of MnSOD reduces diabetic cardiomyopathy. *Diabetes* 55:798-805, 2006
48. Stearns SB: Carnitine content of skeletal and cardiac muscle from genetically diabetic (db/db) and control mice. *Biochem Med* 29:57-63, 1983
49. Semeniuk LM, Kryski AJ, Severson DL: Echocardiographic assessment of cardiac function in diabetic db/db and transgenic db/db-hGLUT4 mice. *Am J Physiol Heart Circ Physiol* 283:H976-982, 2002
50. Yue P, Arai T, Terashima M, Sheikh AY, Cao F, Charo D, Hoyt G, Robbins RC, Ashley EA, Wu J, Yang PC, Tsao PS: Magnetic resonance imaging of progressive cardiomyopathic changes in the db/db mouse. *Am J Physiol Heart Circ Physiol* 292:H2106-2118, 2007
51. Van den Bergh A, Flameng W, Herijgers P: Type II diabetic mice exhibit contractile dysfunction but maintain cardiac output by favourable loading conditions. *Eur J Heart Fail* 8:777-783, 2006

Table I Contractile parameters, myocardial oxygen consumption (MVO_2) and cardiac efficiency (CE) in Langendorff-perfused wild-type and *db/db* mouse hearts.

	GLUCOSE		**GLUCOSE + PALMITATE**	
	WT (n = 13)	***db/db* (n = 13)**	**WT (n = 6)**	***db/db* (n = 6)**
Wet heart weight (g)	0.14 ± 0.01	0.13 ± 0.003	0.12 ± 0.003	0.12 ± 0.04
Heart rate (beats/min)	362.3 ± 3.6	358.4 ± 5.3	364 ± 0.9	355.5 ± 7.6
End diastolic pressure (mmHg)	10.9 ± 0.9	12.5 ± 1	12.9 ± 2.8	13.4 ± 1.9
End systolic pressure (mmHg)	69.9 ± 2.1	60 ± 3.8*	57.2 ± 3.1†	44.9 ± 3.7*†
Developed pressure (mmHg)	58.9 ± 2.2	47.5 ± 3.3*	44.3 ± 4.8†	31.4 ± 3.9*††
Rate pressure product x 10^3 (mmHg/min)	21.4± 0.9	17 ± 1.2*	16.1 ± 1.7†	11.2 ± 1.4*†
dP/dt min (mmHg/s)	2408.5 ± 115.3	2124.4 ± 155.9	2133.7 ± 64.2	1846.3 ± 97.8
dP/dt max (mmHg/s)	2830.2 ± 118.8	2608.5 ± 174.4	2695 ± 98.3	2299.8 ± 132.8
Coronary flow (ml/min)	1.3 ± 0.07	1.4 ± 0.11	1.8 ± 0.15††	1.5 ± 0.14
MVO_2 (µmol/min/g)	23.6 ± 1.5	23.9 ± 1.8	17.3 ± 1.6†	25 ± 2.8*
% Cardiac efficiency	28 ± 1.9	22.8 ± 2.7 #	28.6 ± 3.3	14.1± 2.3**†

Values are means ± SEM. *$p < 0.05$; ** $p < 0.005$ *versus* wild-type under the same perfusion conditions; †$p < 0.05$; ††$p < 0.005$ *versus* glucose. # $p < 0.05$ versus wild-type under the same perfusion condition with Mann Whitney test.

FIGURE LEGENDS

Figure 1. Increased mitochondrial proliferation in *db/db* hearts. (**A**), Representative electron micrographs from wildtype (**a** and **c**) and *db/db* (**b** and **d**) hearts. The magnification in (**a**) and (**b**) is X2000 and in (**c**) and (**d**) is X8000. The arrows show lipid droplets and "**M"** represents mitochondria. (**B**), Mitochondrial number obtained by blind counting of three equivalent sections from each of three separate hearts in each group (wildtype or *db/db*). (**C**), Mitochondrial DNA relative to nuclear DNA represented as fold change compared to wildtypes, arbitrarily defined as 1. Data were obtained from 5 wildtypes and 6 *db/db* mice performed in triplicate. Data are means ± SEM. * $p < 0.05$, ** $p < 0.005$ *versus* wildtype.

Figure 2. Increased oxidative stress in *db/db* hearts. (**A**), H_2O_2 production in isolated mitochondria from wildtype and *db/db* hearts (n = 6 hearts per genotype). H_2O_2 production was measured under state 4 conditions (in the presence of 1 μg/ml oligomycin) with succinate (4 mmol/L) and rotenone (10 μmol/L). [a] $p < 0.04$ *versus* WT treated with oligomycin alone; [b] $p < 0.05$ *versus* similarly treated WT, [c] $p < 0.05$ *versus db/db* treated with oligomycin alone; [d] $p < 0.03$ *versus db/db* treated with succinate. (**B**), Malondialdehyde (MDA) levels in wildtype and *db/db* heart homogenates (n = 6 hearts per genotype performed in triplicate). (**C**), Representative western-blots and the corresponding densitometry for 4-hydroxynonenal (4-HNE) protein adducts and MnSOD in wildtype and *db/db* hearts. These blots were normalized to α-tubulin (bottom). Densitometry is based on 7 wildtypes and 6 *db/db* hearts performed in duplicate. Wildtypes are represented by open bars and the *db/db* by black bars. Data represent means ± SEM. * $p < 0.05$; ** $p < 0.005$ *versus* wildtype controls.

Figure 3. Mitochondrial function studied in saponin-permeabilized cardiac fibers obtained from glucose-perfused *db/db* and wildtype (WT) hearts**.** (**A**), Glutamate-malate respiration. State 2 (V_0) corresponds to respiration in the presence of substrate; state 3 (V_{ADP}) is respiration in the presence of substrate plus 1 mmol/L exogenous ADP; state 4 (V_{Oligo}) corresponds to respiration in the absence of ATP synthesis using 1 μg/ml oligomycin to inhibit ATP synthase, RC is the respiratory control ratio (V_{ADP}/V_{Oligo}). (**B**), Pyruvate-malate respiration. (**C**), Palmitoyl-carnitine (PC)-malate respiration. (**D**, **E** and **F**), ATP synthesis rates and ATP/O ratios in glutamate, pyruvate and PC respiring fibers respectively. Data are obtained from 4 hearts per genotype for glutamate and pyruvate and from 5 hearts per genotype for PC. (**G**), Representative western-blot and the corresponding densitometry for the subunit α of the F1 complex of the ATP synthase protein (complex V). The blots were normalized to complex II protein, which was unchanged between the two genotypes (n = 3 hearts per genotype). Data represent means ± SEM. * $p < 0.05$; ** $p < 0.005$ *versus* wildtype controls.

Figure 4. FA-induced mitochondrial uncoupling in *db/db* hearts. (**A**), State 3 (V_{ADP}), (**B**), State 4 (V_{Oligo}), (**C**), ATP and (**D**), ATP/O ratios in glucose and glucose + palmitate perfused wildtype (□ ,⊡) and *db/db* (■ , ▩) hearts. The respirations were performed on saponin-permeabilized cardiac fibers in the presence of palmitoyl-carnitine-malate.

Data represent means ± SEM. * $p < 0.05$; ** $p < 0.005$ *versus* wildtype under the same perfusion conditions; $^{\dagger}p < 0.05$ *versus* glucose, (n = 6 hearts per genotype).

Figure 5. Mitochondrial uncoupling in wildtype and *db/db* mitochondria. Respiration rates were measured in saponin-permeabilized cardiac fibers and proton leak kinetics were measured in isolated mitochondria obtained from wildtype and *db/db* hearts that were perfused with 11 mmol/L glucose and 1 mmol/L palmitate for 20 minutes. **(A)**, Respiration rates in saponin-permeabilized cardiac fibers from wildtype (blue) and *db/db* (red) hearts. Respirations were carried under state 4 conditions (presence of 1μg/ml oligomycin) with succinate (4 mmol/L) and rotenone (10 μmol/L). GDP (500 μmol/L) alone followed by addition of atractyloside (ATR) (5 μmol/L) were used to inhibit uncoupling proteins or ANT respectively. (n = 9 hearts per genotype). *$p < 0.05$ *versus* equivalently treated wildtype; $^{\#}p < 0.005$ *versus* oligomycin + succinate + rotenone; $^{+}p = 0.07$ *versus* GDP. **B,** Proton leak kinetics in isolated mitochondria from wildtype under control conditions (absence of GDP and ATR, black circles); in the presence of GDP alone (Blue squares) and in the presence of both GDP and ATR (green triangle). **C,** same as **B** but represents proton leak in *db/db*. **D**, **E** and **F** are proton leak kinetics in wildtype (in blue) and *db/db* in red under control conditions, with GDP alone or with GDP + ATR respectively. Data are means ± SEM. (n = 4-6 hearts per genotype). Standard error bars are removed for clarity. The mean and SEM values used to generate these curves are shown in supplementary table S2.

Figure 6. UCP 3 and ANT1 protein expression in wildtype and *db/db* hearts. **A**, Representative western-blot and the densitometry analysis for UCP 3 protein in total heart extracts isolated from wildtype (n = 7), *db/db* (n = 8) and one UCP 3 KO mouse. Coomassie blue staining of the corresponding gel was used as a loading control. **B**, Representative western-blot and the densitometry analysis for ANT1 protein in total heart extracts isolated from wildtype (n = 7), *db/db* (n = 8) and one muscle specific ANT1KO and an ANT1 wildtype littermate. Coomassie blue staining of the corresponding gel was used as a loading control. Data represent mean ± SEM. *$p < 0.05$ *versus* wildtype.

Figure 7. Relative gene expression. mRNA from six wildtype and six *db/db* hearts were amplified by real-time PCR and normalized to lamin A expression. Values represent fold change in mRNA transcript levels relative to wildtype, which was assigned as 1. Data represent mean ± SEM * $p < 0.05$; ** $p < 0.005$ *versus* wildtype controls. $^{\#}p = 0.07$ *versus* wildtype. Full gene names as well as primers used are listed in supplementary table S1.

Figure 1

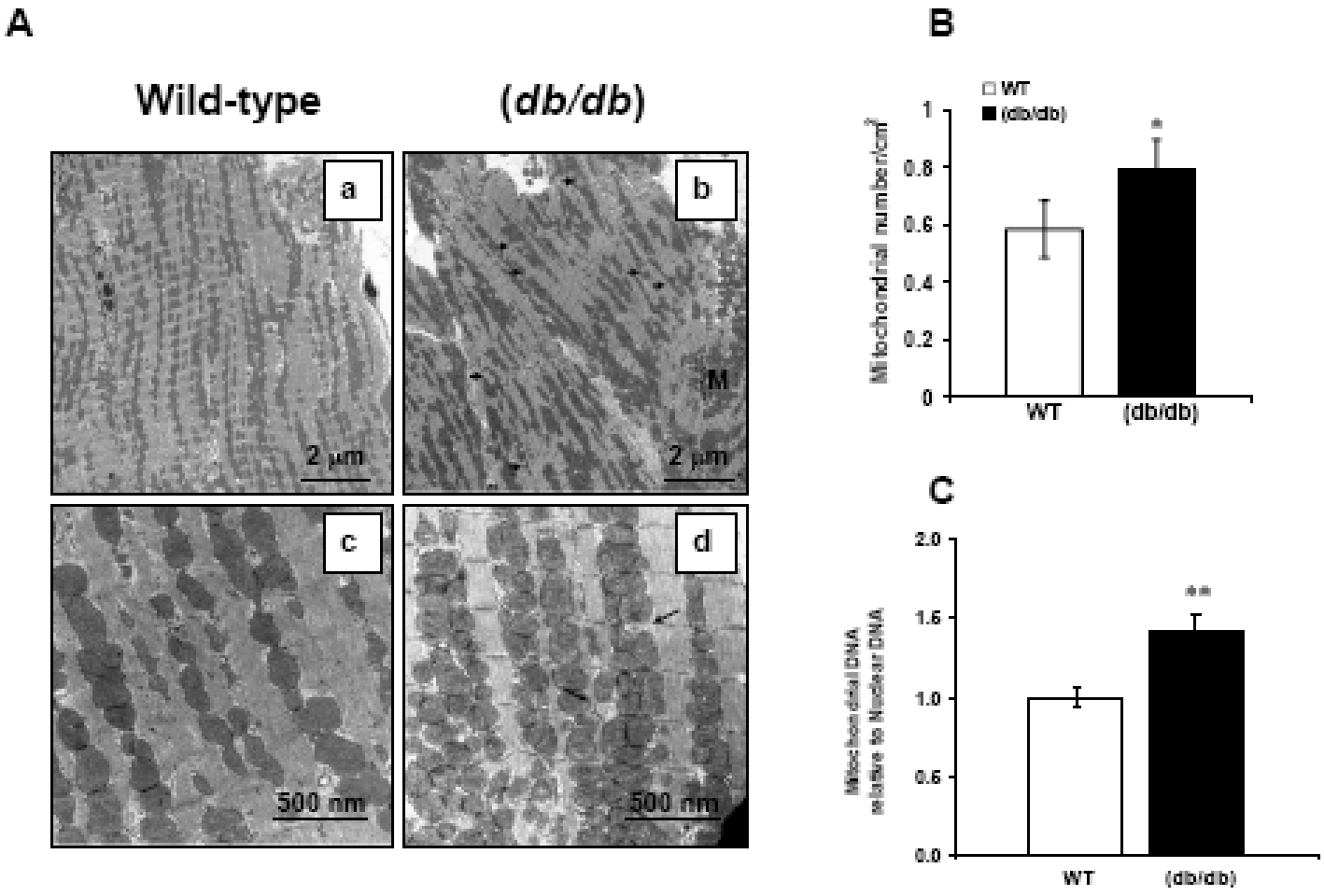
A
Wild-type
(db/db)
a
b
c
d
2 μm
2 μm
500 nm
500 nm
M
B
WT
(db/db)
Mitochondrial number/cm²
1
0.8
0.6
0.4
0.2
0
*
WT
(db/db)
C
2.0
1.6
1.0
0.6
0.0
**
WT
(db/db)

Figure 2

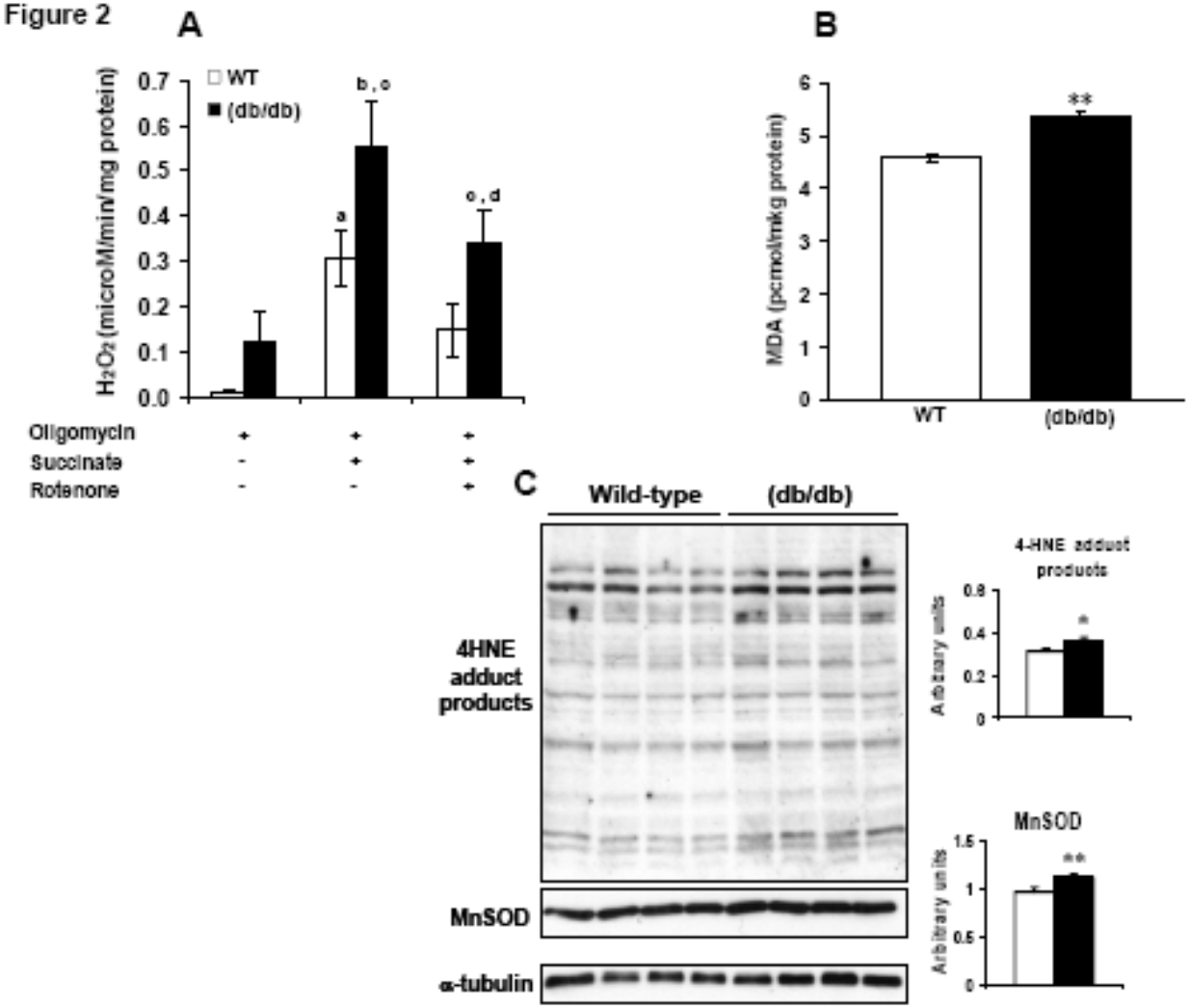
A
B
C
WT
(db/db)
H_2O_2 (microM/min/mg protein)
0.7
0.6
0.5
0.4
0.3
0.2
0.1
0.0
a
b , c
c , d
Oligomycin
Succinate
Rotenone
MDA (pcmol/mkg protein)
6
5
4
3
2
1
0
**
WT
(db/db)
Wild-type
(db/db)
4HNE adduct products
MnSOD
α-tubulin
4-HNE adduct products
Arbitrary units
0.8
0.4
0.2
0
*
MnSOD
Arbitrary units
1.5
1
0.5
0
**

Figure 3

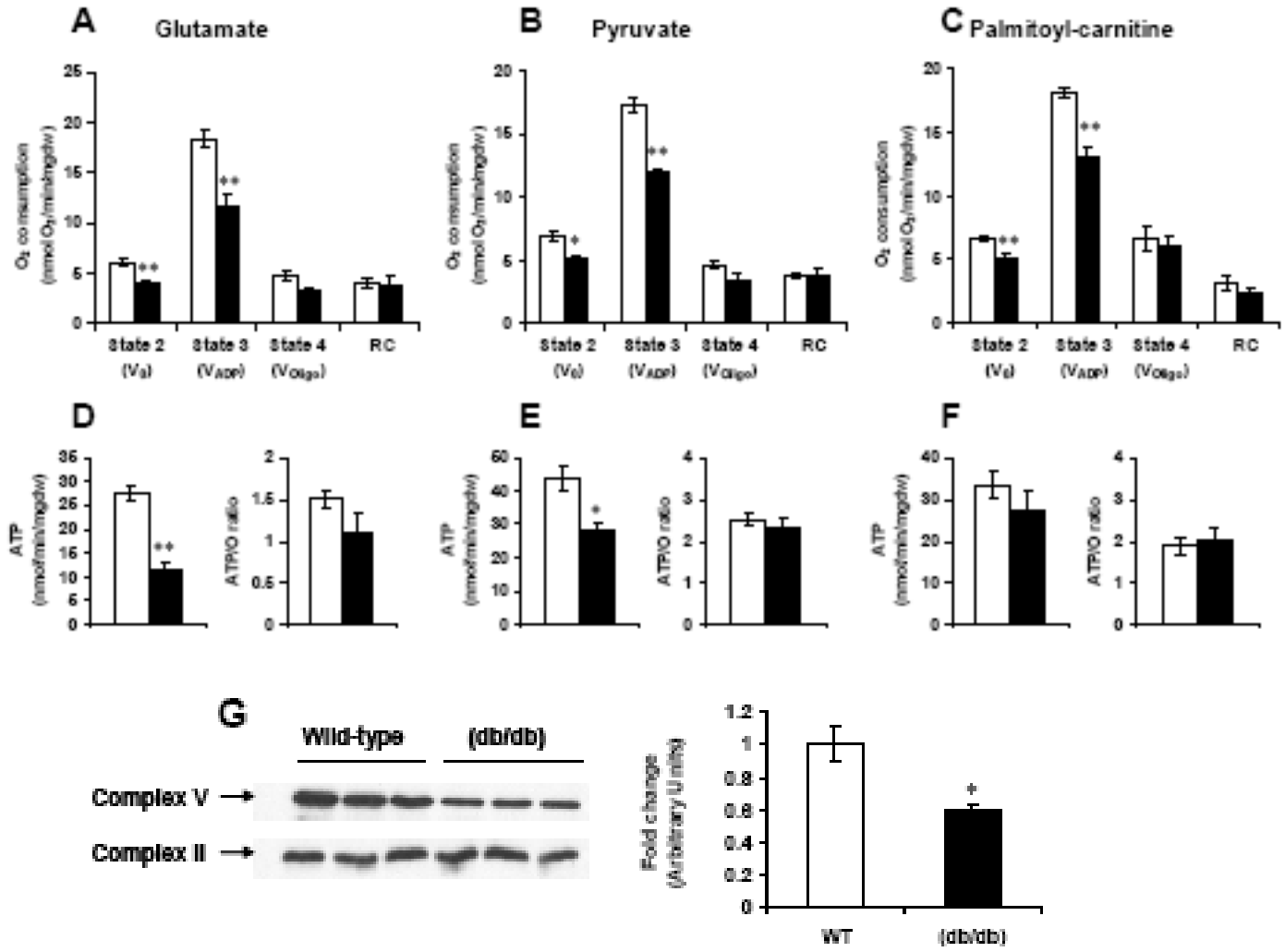
A
Glutamate
B
Pyruvate
C
Palmitoyl-carnitine
State 2
State 3
State 4
RC
D
E
F
ATP
ATP/O ratio
G
Wild-type
(db/db)
Complex V
Complex II
Fold change
WT
(db/db)

Figure 4

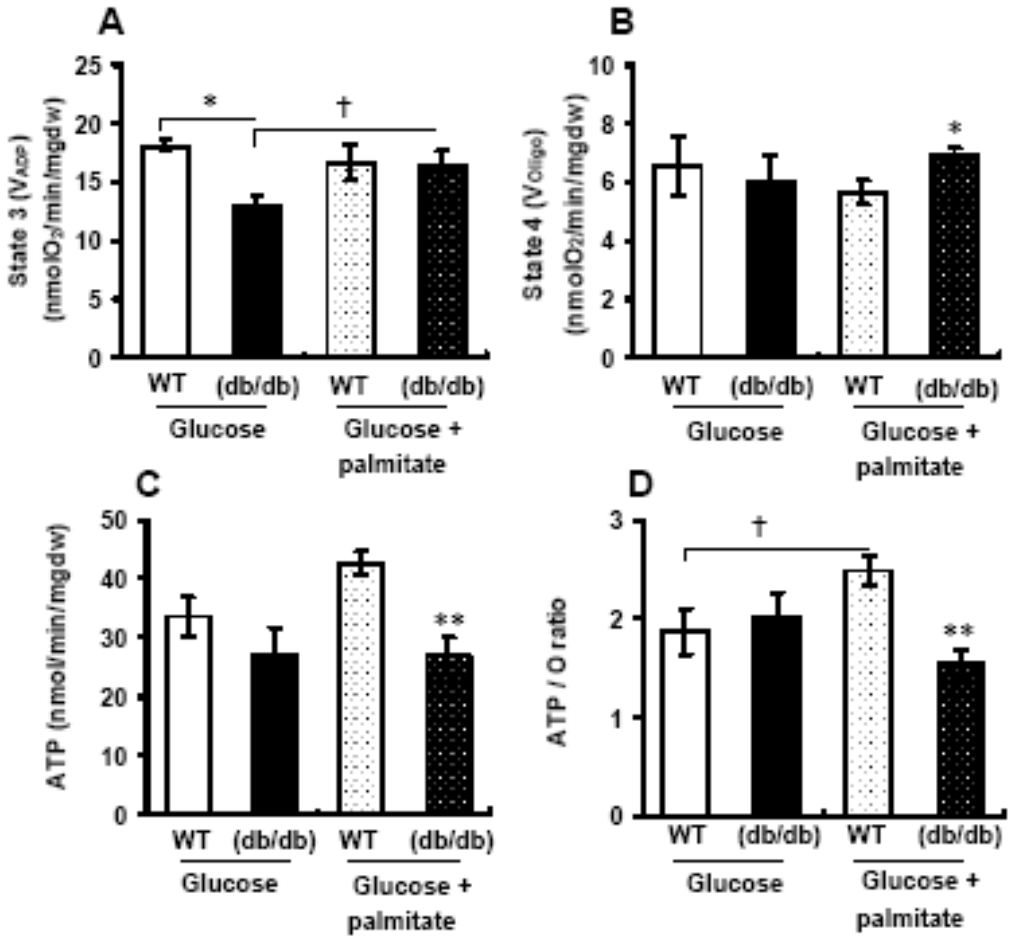
A
State 3 (V_{ADP}) (nmolO_2/min/mg dw)
25
20
15
10
5
0
*
†
WT
(db/db)
WT
(db/db)
Glucose
Glucose + palmitate
B
State 4 (V_{Oligo}) (nmolO_2/min/mg dw)
10
8
6
4
2
0
*
WT
(db/db)
WT
(db/db)
Glucose
Glucose + palmitate
C
ATP (nmol/min/mg dw)
50
40
30
20
10
0
**
WT
(db/db)
WT
(db/db)
Glucose
Glucose + palmitate
D
ATP / O ratio
3
2
1
0
†
**
WT
(db/db)
WT
(db/db)
Glucose
Glucose + palmitate

Figure 5

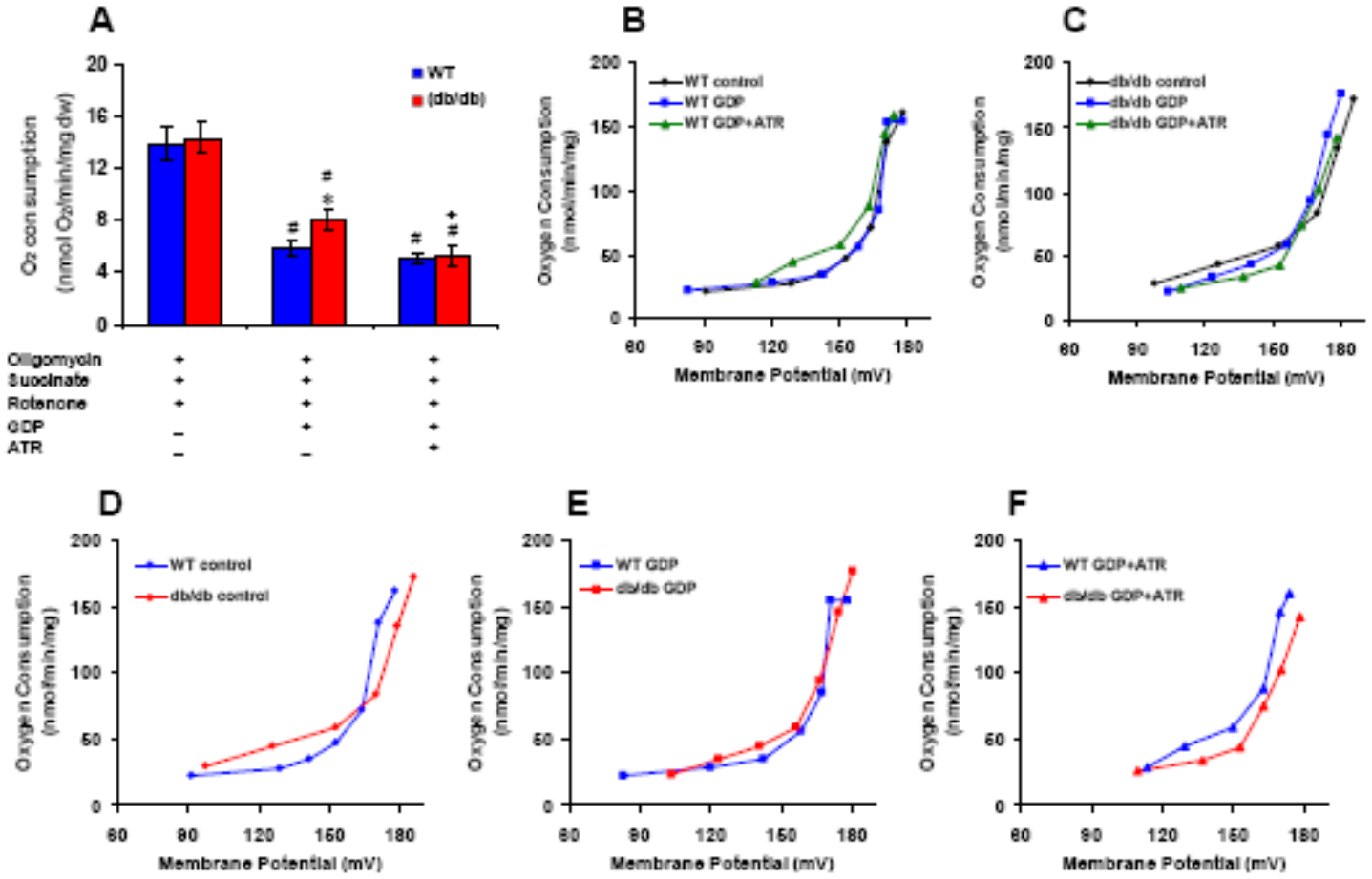
A
B
C
D
E
F
WT
(db/db)
O2 consumption (nmol O2/min/mg dw)
Oligomycin
Succinate
Rotenone
GDP
ATR
WT control
WT GDP
WT GDP+ATR
db/db control
db/db GDP
db/db GDP+ATR
Oxygen Consumption (nmol/min/mg)
Membrane Potential (mV)

Figure 6

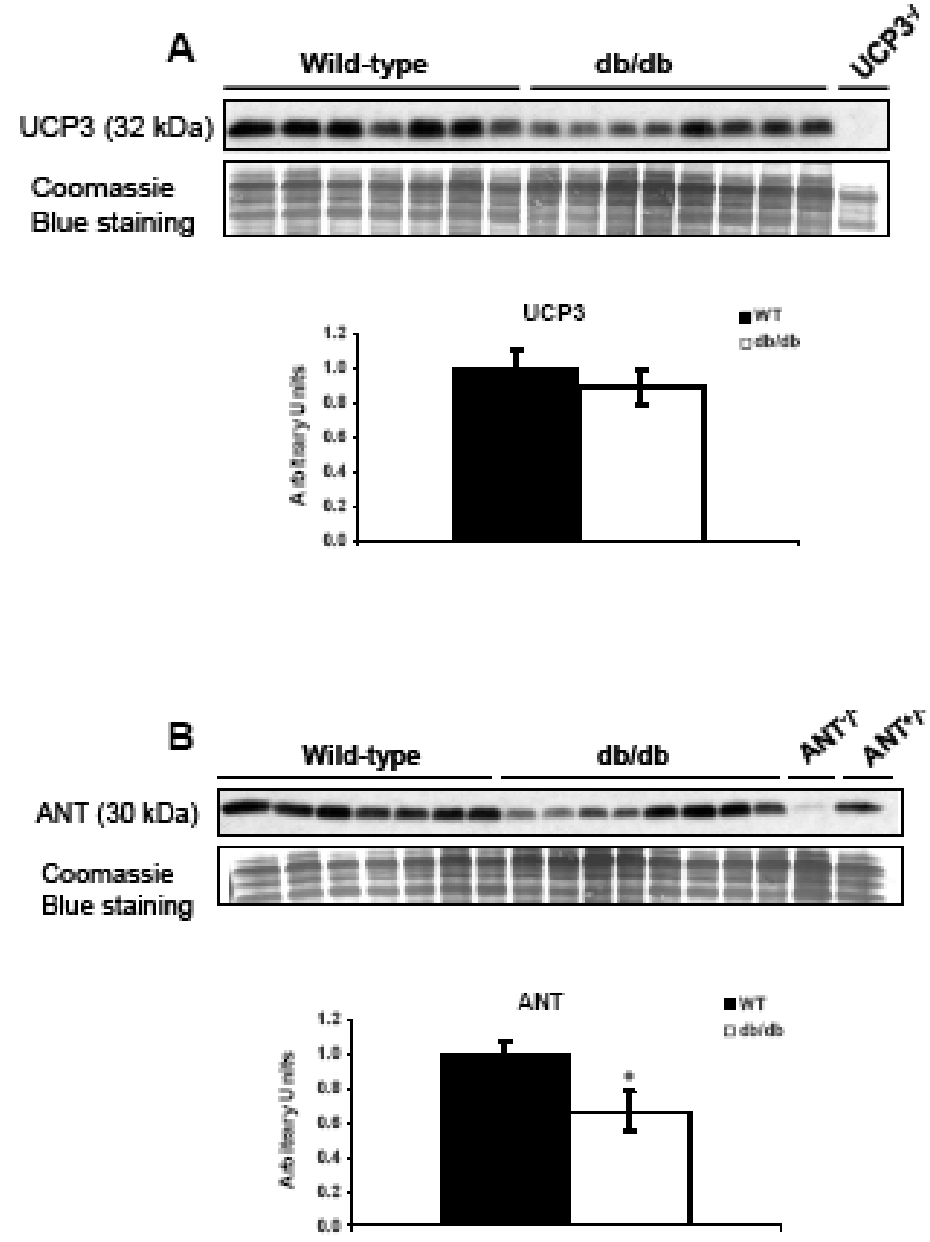
A
Wild-type
db/db
UCP3-/-
UCP3 (32 kDa)
Coomassie
Blue staining
UCP3
WT
db/db
Arbitrary Units
1.2
1.0
0.8
0.6
0.4
0.2
0.0
B
Wild-type
db/db
ANT-/-
ANT-/-
ANT (30 kDa)
Coomassie
Blue staining
ANT
WT
db/db
*
Arbitrary Units
1.2
1.0
0.8
0.6
0.4
0.2
0.0

Figure 7

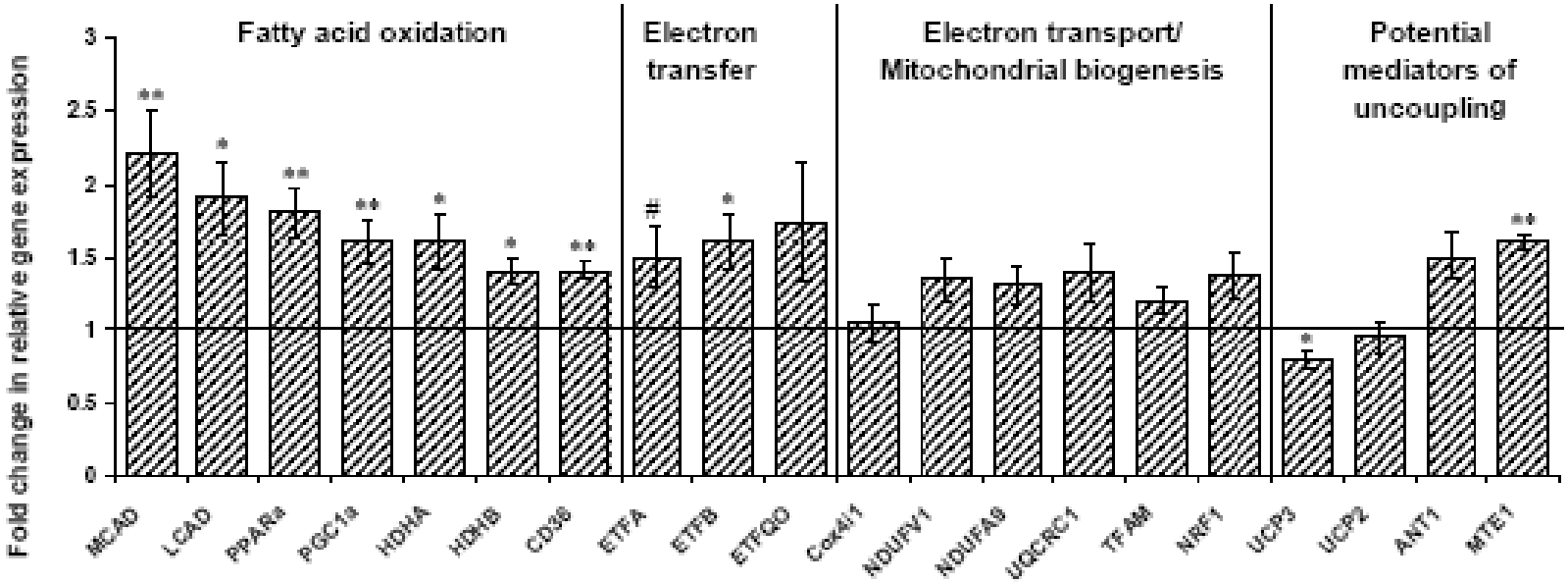
Fatty acid oxidation
Electron transfer
Electron transport/ Mitochondrial biogenesis
Potential mediators of uncoupling
Fold change in relative gene expression
3
2.5
2
1.5
1
0.5
0
MCAD
LCAD
PPARa
PGC1a
HDHA
HDHB
CD36
ETFA
ETFB
ETFQO
Cox4i1
NDUFV1
NDUFA9
UQCRC1
TFAM
NRF1
UCP3
UCP2
ANT1
MTE1